Degradation of ferroelectric and weak ferromagnetic properties of $BiFeO_3$ films due to the diffusion of silicon atoms*

Xiao Ren-Zheng(肖仁政)[a], Zhang Zao-Di(张早娣)[a], Vasiliy O. Pelenovich[b], Wang Ze-Song(王泽松)[a], Zhang Rui(张 瑞)[a], Li Hui(李 慧)[a], Liu Yong(刘 雍)[a], Huang Zhi-Hong(黄志宏)[a]†, and Fu De-Jun(付德君)[a]‡

[a] *Key Laboratory of Artificial Micro- and Nano-Materials of Ministry of Education, School of Physics and Technology, Wuhan University, Wuhan* 430072, *China*

[b] *Department of Physics and Technology, Huazhong Normal University, Wuhan* 430070, *China*

(Received 2 December 2013; revised manuscript received 31 December 2013; published online 28 May 2014)

Crystalline $BiFeO_3$ (BFO) films each with a crystal structure of a distorted rhombohedral perovskite are characterized by X-ray diffraction (XRD) and high-resolution electron microscopy (HRTEM). The diffusion of silicon atoms from the substrate into the $BiFeO_3$ film is detected by Rutherford backscattering spectrometry (RBS). The element analysis is performed by energy dispersive X-ray spectroscopy (EDS). Simulation results of RBS spectrum show a visualized distribution of silicon. X-ray photoelectron spectroscopy (XPS) indicates that a portion of silica is formed in the diffusion process of silicon atoms. Ferroelectric and weak ferromagnetic properties of the BFO films are degraded due to the diffusion of silicon atoms. The saturation magnetization decreases from 6.11 down to 0.75 emu/g, and the leakage current density increases from 3.8×10^{-4} up to 7.1×10^{-4} A/cm^{-2}.

Keywords: ferroelectric, ferromagnetic, diffusion, silicon

PACS: 75.50.Gg, 77.80.–e, 68.35.Fx, 82.80.Yc **DOI:** 10.1088/1674-1056/23/7/077504

1. Introduction

$BiFeO_3$ (BFO) film has a crystal structure of a distorted rhombohedral perovskite (space group $R3c$).[1] Such a symmetry allows the coexistence of two orders: ferroelectricity and antiferromagnetism with rather superior ordering temperatures of 1143 K and 643 K, respectively.[2–5] A linear coupling behavior between magnetization and electric polarization shows that the spontaneous polarization and spontaneous magnetization can be switched under applied electric and magnetic fields.[6,7] This indicates that multiferroic materials have great potentials for practical applications in spintronics devices, various sensors, data-storage media, and multiple-state memories.[8,9]

Although BFO has attracted great attention due to its extensive application prospects and interesting physics as well, there remain several obstacles to be solved before its practical applications in multiferroic devices at room temperature, such as small spontaneous polarization (P_s), remnant polarization (P_r),[10,11] high coercive field,[12,13] ferroelectric reliability,[14] inhomogeneous magnetic spin structure,[15] and high leakage current.[16,17] First-principles studies of spontaneous polarization predict a large ferroelectric polarization of 90–100 C/cm^2 in multiferroic BFO along the [111] direction.[18] However, the large polarization is hardly achieved and has been obtained by a few groups in the pure phase $BiFeO_3$ as reported by Wang *et al.*[8] in epitaxial BFO multiferroic film and Lebeugle *et al.*[19] in BFO single crystals. Actually, the reason has been confirmed that serious leakage current leads to the restriction on device application of BFO. The major contribution to leakage current is attributed to a small number of Fe^{2+} ions and oxygen vacancies existing in BFO material.[10,13] Therefore, it is crucial to study the mechanism of leakage current and even more important is how to reduce it. Much work in this respect has been done and obvious consequences on the leakage mechanism have been obtained.[4,20] Numerous countermeasures have been actualized to reduce the leakage current and enhance the ferroelectricity of BFO.[9,13] On the other hand, the enhanced ferromagnetism is also an essential study subject.[16]

Rutherford backscattering spectrometry (RBS) is one of the most vital tools of ion beam analysis. It possesses high mass and depth resolution, thus it has a significant advantage in the study of diffusion issues. The interface reaction and diffusion of silicon atoms from the substrate into the films have been reported by Huang and Shannigrahi[21] and Kogut and Record.[22] The phenomenon of substrate silicon atom diffusion into the BFO film has been observed in our experiment when RBS is used to probe the depth profile of silicon, and then it is anticipated that the physical properties of the BFO films would be affected by the diffusion of silicon atoms. If the anticipation turns out to be true, such a diffusion would become an important factor that influences the physical properties of BFO films. Therefore, in this study, several samples with different annealing times and temperatures are synthesized. The purpose of the study is to prove the supposition

*Project supported by the International Cooperation Program of the Ministry of Science and Technology of China (Grant No. 2011DFR50580) and the National Natural Science Foundation of China (Grant Nos. 11105100, 11205116, and 11350110206).

†Corresponding author. E-mail: hzh19790109@126.com

‡Corresponding author. E-mail: djfu@whu.edu.cn

© 2014 Chinese Physical Society and IOP Publishing Ltd

that the physical properties of BFO films can be affected by the diffusion of silicon atoms from the substrate.

2. Experimental procedure

BFO films were prepared by the sol–gel technique using ferric nitrate ($Fe(NO_3)_3{\cdot}9H_2O$) and bismuth nitrate ($Bi(NO_3)_3{\cdot}5H_2O$) as precursors. N-type Si (100) with resistivity value of 2 Ω·cm was used as the substrate. The films were prepared on Si (100) substrates by spin coating four times with 5000 rpm and subsequently annealed at different temperatures for a dwell time. A series of samples was made through different annealing processes from room temperature to 650 °C. A few of them each with a good crystallinity and pure phase BFO film were obtained through an annealing process first at 350 °C for 5 min and then at 550 and 600 °C for 5–10 min.

The crystal structures of the films were characterized by X-ray diffraction (XRD) and high-resolution electron microscopy (HRTEM). The thickness values of the films were measured by Scanning electron microscopy (SEM). The concentrations of all elements in the cross sections of the films were detected by energy dispersive X-ray spectroscopy (EDS). The depth profiles of all elements in the films associated with the atomic diffusion induced thermodynamically were investigated by RBS. The ferromagnetic properties of the BFO films were obtained by vibrating sample magnetometry (VSM) with the magnetic field in the direction parallel to the film surface. The ferroelectric hysteresis loops of the films were studied using a commercial ferroelectric tester (Radiant Technologies) and the leakage current was measured by an Agilent 4155C Semiconductor Analyzer. Elementary chemical environment analyses of BFO films were characterized by X-ray photoelectron spectroscopy (XPS). The instrument model of the XPS is an ESCLAB 250Xi. The source of XPS is Al–K_α with an energy of 1486.68 eV.

3. Results and discussion

Figure 1 shows XRD spectra of the samples S1, S2, and S3. No impurities are found in the $BiFeO_3$ films annealed for 5 and 10 min at 550 °C and for 10 min at 600 °C, these films are denoted as S1, S2, and S3, respectively. The crystal structures of the samples S1, S2, and S3 are of distorted rhombohedral perovskite (*R*3*c* space group, ICSD 86-1518). Below we can confirm that the silicon atoms diffuse into the film from the substrate and that a portion of them generate silica. In addition, no crystallization peaks of silicon and silica can be found in Fig. 1.

The Rutherford backscattering spectra of Si (100), S1, S2, and S3 samples shown in Fig. 2 are studied by 2.72 MeV Li^{2+} ions obtained from a source of negative ions by cesium sputtering (SNICS) and 2 ×1.7 MV tandem accelerator at a scattering angle of 165° with Au–Si surface barrier detector. A series of information can be obtained from Fig. 2. The peaks of O, Si, Fe, and Bi can be observed clearly in Fig. 2 from the locations of the signal determined by the kinematic factor $\boldsymbol{k}$ of the elements. The peak of the element located on the right-hand side in the RBS spectra corresponds to a larger kinematic factor. The RBS spectrum of the Si (100) is tested as a standard spectrum for comparison with the spectra of other samples to prove the diffusions of silicon atoms occurring in the films. The location of O peak between channels 44–72 in RBS has not been considered here because its signal is superimposed upon the signal of silicon and it has a slight scattering cross section which can bring to a large statistical error. The height of the flattop of silicon peak in RBS spectrum is proportional to the energy loss, which increases with the augment of thickness of the film due to the scattering cross section depending on the energy (E) of the impinging projectile as E^{-2}. The front edge of the silicon peak rises slowly with annealing time and temperature increasing, indicating that the diffusion of silicon atoms from the substrate Si (100) into the film increases with annealing time and temperature rising. The result can be proved by EDS measurement near the surface of the film (the sample S2) (Fig. 3(a)). Figure 3(a) shows that an amount of the silicon content is about 23 wt% among Bi, Fe, O, and Si elements. The signal of copper in EDS (Fig. 3(a)) originates from the copper ring used to support the sample in process of HRTEM measurement. The RBS spectra of the samples S1, S2, and S3 are simulated by the SIMNRA software. Dots and lines represent experimental data and simulated shape, respectively (see Fig. 2). SEM surface morphology and cross section image of the sample S2 are shown in Figs. 4(a) and 4(b). SEM measured thickness values of the films S1, S2, and S3 are all about 160 nm. The simulated line matches perfectly with the experimental data. The relations between the silicon atom concentration and depth for films S1, S2, and S3 are shown in Fig. 3(b). Figure 3(b) shows that the thermal diffusion of silicon atoms from the substrate into the film is not a linear process. The nonlinear changes of atom concentration gradient can be explained by the fact that oxidation helps the Si atom migration in the BFO film and diffusion of silicon atoms in the film is restrained after self-interstitial saturation of Si atoms.[24,25]

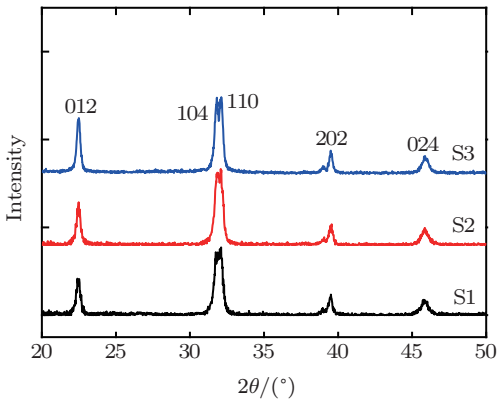


Fig. 1. (color online) X-ray diffraction patterns of the pure phase $BiFeO_3$ thin films S1, S2, and S3.

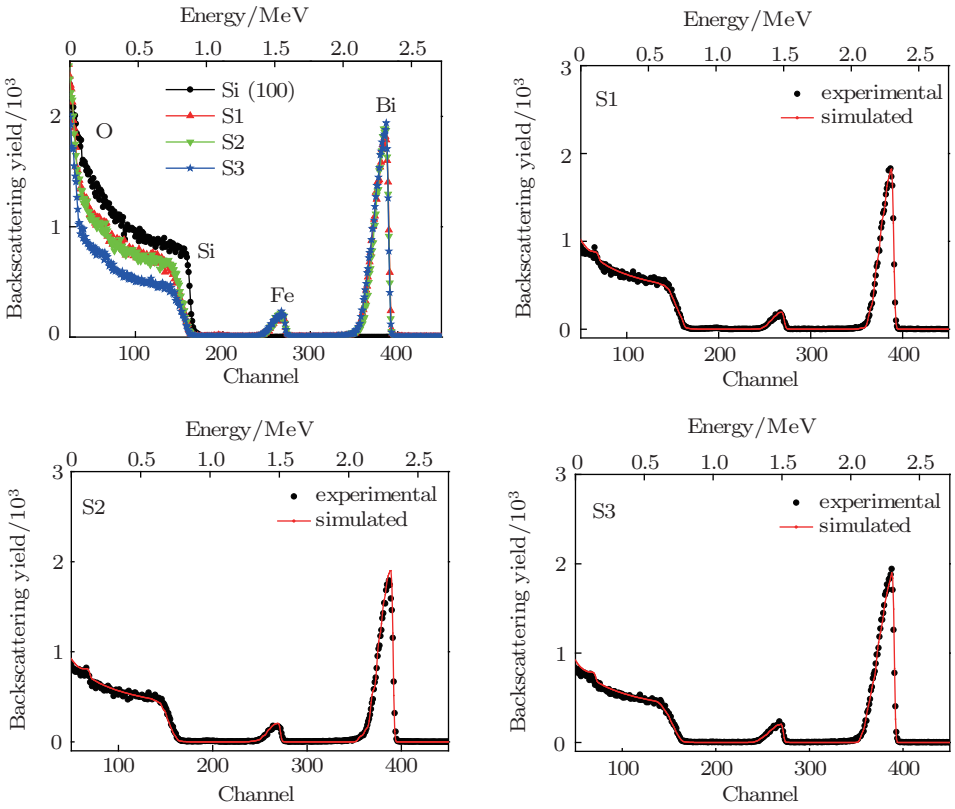


Fig. 2. (color online) (a) Rutherford backscattering spectra of Si (100), S1, S2, and S3. The RBS spectra of samples (b) S1, (c) S2, and (d) S3 are fitted by the SIMNRA software.

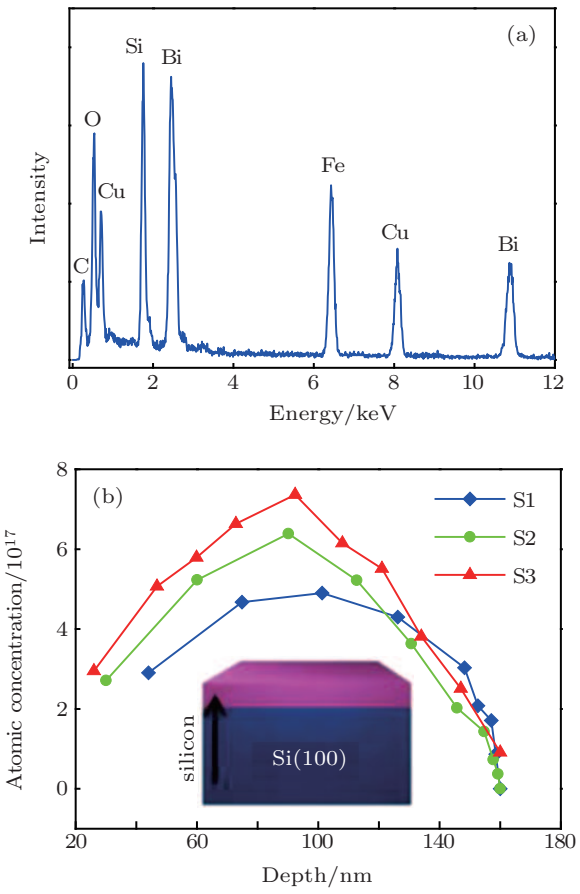


Fig. 3. (color online) (a) Energy dispersive X-ray spectra of the S2 sample cross section. (b) The relevant curves of atomic concentration of silicon change with depth distribution in the films of samples S1, S2, and S3.

The crystalline nature of the pure phase $BiFeO_3$ film (the sample S2) in cross section image is confirmed by high resolution transmission electron microscopy (Fig. 4(d)). Figure 4(c) shows the Si/$BiFeO_3$ interface. The crystallization area in Fig. 4(d) undisputedly belongs to BFO, and the ownership of the amorphous part shown in the image needs to be discussed in detail. A reasonable assumption could be made. If the amorphous composition belongs to silicon or silica, the result of EDS in the area should be an intense peak of silicon, however the result has revealed that only about 20 wt% of silicon exists in this place and similar to the proportion of silicon in the crystalline regions of BFO, which means that the amorphous part derives from BFO and implies that the silicon and silica exist in the films in a free form. The EDS measurement is performed from the HRTEM cross section by using an electron beam with a diameter of 50 nm. The relative error is about 1.76% for the Bi element, 1.52% for the Fe element, and 1.49% for the Si element in Fig. 3(a). The information about the crystal structure of the sample and the diffusion of silicon atoms is analyzed via the description above in this paper. The silicon chemical environment analyses on the pending issues are implemented by XPS. The XPS spectra of the Si 2p shown in Fig. 5(a) can be well fitted by four chemical states. The binding energies of fitted peaks are 99.5 eV, 100.0 eV,

103.0 eV, and 103.7 eV respectively. These data can be confirmed if the spectroscopic peak located at 99.5 eV is attributed to photoemission from SiO_2/Si,[26] the peak at 100.0 eV is ascribed to the photoemission from Si $2p_{3/2}$,[27] the peak at 103.0 eV stems from the photoemission from SiO_2 $2p_{3/2}$,[28] and the peak at 103.7 eV arises from the photoemission from SiO_2 $2p_{1/2}$.[29,30] The existence of the chemical bonds Si–O and SiO_2/Si in XPS spectra illustrates that a portion of silicon atoms react with oxygen atoms to form silica with the spread of silicon atoms.

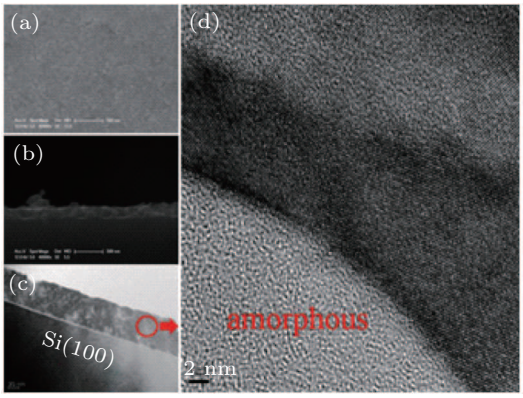


Fig. 4. (color online) (a) SEM surface morphology, (b) SEM cross section image, (c) HRTEM image and of (d) the sample S2.

The magnetizations of the BFO films S1, S2, and S3 each as a function of external magnetic field in a range of −5–5 kOe are shown in Fig. 5(b). Magnetization is measured directly for the film on the Si (100) substrate. Then the magnetization of the substrate is subtracted. The magnetic field is applied in the direction parallel to the film plane. Hysteresis loops as the characteristic of a weak ferromagnetism are clearly observed (see the inset in Fig. 5(b)). The saturation magnetizations are 6.11, 2.59, and 0.75 emu/g, the remnant magnetizations are 0.15, 0.21, and ∼ 0 emu/g, and the coercive fields are 22.7, 72.6, and ∼ 0 Oe for the samples S1, S2, and S3, respectively. It is well known that the saturation magnetization is one of the principal yardsticks of magnetic materials. It is clear that the weak ferromagnetism of the films degenerates with the increases of annealing time and temperature. That means that a decrease of the saturation magnetization of the sample is possible, owing to the diffusion of silicon atoms in the film. It is well known that the magnetic properties of $BiFeO_3$ originate from partially filled d orbitals of Fe^{3+} ions and each Fe^{3+} spin is surrounded by six antiparallel spins on the nearest Fe neighbors. The super exchange and spin-orbit interaction of Fe^{3+}–O–Fe^{3+} or Fe^{3+}–O–Fe^{2+} is the source of antiferromagnetic property of BFO.[5] Therefore, the decrease of saturation magnetization caused by diffusion of silicon atoms may be explained by formative silica due to its snatching of oxygen atoms of BFO and disturbed the super exchange between Fe atoms and O atoms.

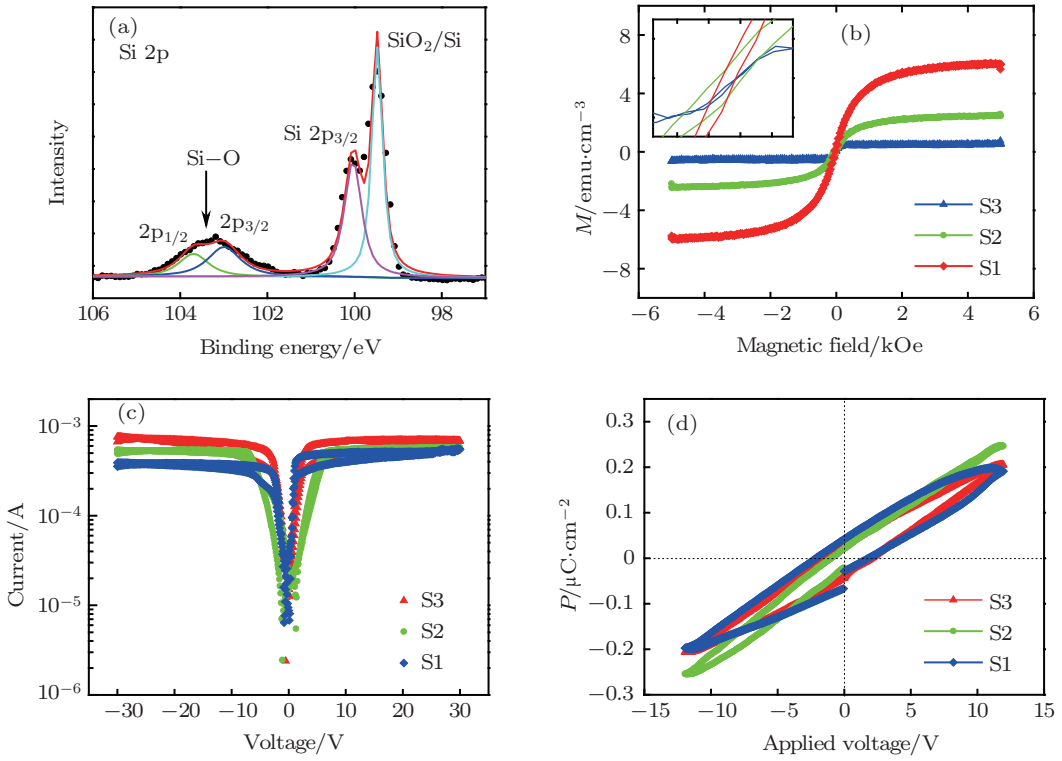


Fig. 5. (color online) (a) X-ray photoelectron spectrum of sample S2 in cross-section. (b) Magnetic hysteresis loops, (c) *I*–*V* curves, and (d) *P*–*V* curves of the $BiFeO_3$/Si (100) thin films S1, S2, and S3.

The measured leakage currents and ferroelectric hysteresis loops of the thin films are shown in Figs. 5(c) and 5(d) respectively. Each of the films shows a larger leakage current under the applied voltage (Fig. 5(c)). Figure 5(d) shows the ferroelectric hysteresis loops of the thin films measured using a commercial ferroelectric tester (Radiant Technologies) at an applied voltage of 12 V of 1 kHz. The leakage current densities at an applied voltage of 30 V are 3.8×10^{-4}, 5.4×10^{-4}, and 7.1×10^{-4} A/cm^{-2} for S1, S2, and S3 samples, respectively. The reason why *P*–*E* curves of the thin films cannot reach saturation values can be ascribed to strong leakage current behavior associated with the motion of oxygen vacancies.[10,23] The value of leakage current increases with the increases in annealing time and temperature, and this phenomenon can be correlated with the diffusion process of silicon atoms. The XPS spectra (Fig. 5(a)) of the sample S2 show that a part of silica has been formed with the spread of silicon atoms. Therefore, it is also a possible cause that the formative silica competes with oxygen atoms in BFO and increases concentration of oxygen vacancies in the BFO film, thus resulting in the increase of the leakage current.

4. Conclusions

In this paper, the diffusion of silicon atoms from the substrate into the film is revealed by RBS and EDS measurements. The XPS spectra show a portion of silica formed on the surface of the film. XRD and HRTEM analyses reveal that the diffusion of silicon atoms from the substrate into the film exists in the free state. The leakage current densities under an applied voltage of 30 V are 3.8×10^{-4}, 5.4×10^{-4}, and 7.1×10^{-4} A/cm^{-2} for S1, S2, and S3 samples, respectively. The leakage current increases along with the increases of annealing time and temperature. It can be explained by the diffusion of silicon atoms, which results in the increase of conductivity. A probable reason can be that silica formed in the film increases the number of oxygen vacancies in the film and the value of leakage current. The saturation magnetizations are 6.11, 2.59, and 0.75 emu/g corresponding to the samples S1, S2, and S3, respectively. The diffusion of silicon atoms reduces the saturation magnetization. Such a phenomenon can be explained by formative silica due to its gaining oxygen molecules of $BiFeO_3$ and disturbing the super exchange of Fe^{3+}–O–Fe^{3+} or Fe^{3+}–O–Fe^{2+}, thereby reducing the saturation magnetization of the sample.

References

[1] Kubel F and Schmid H 1990 *Acta Crystallogr. B* **46** 698
[2] Fruth V, Ramer R, Popa M, Calderon-Moreno J M, Anghel E M, Gartner M, Anastasescu M and Zaharescu M 2007 *J. Mater. Sci.: Mater. Electron.* **18** S187
[3] Zou J, Jiang J Z, Zhang Y X, Ma J N and Wan Q J 2012 *Mater. Lett.* **72** 134
[4] Pabst G W, Martin L W, Chu Y H and Ramesh R 2007 *Appl. Phys. Lett.* **90** 072902
[5] Yuan X Y, Luo L R, Wu D and Xu Q Y 2013 *Chin. Phys. B* **22** 107702
[6] Catalan G and Scott J F 2009 *Adv. Mater.* **21** 2463
[7] Fiebig M 2005 *Phys. D: Appl. Phys.* **38** R123
[8] Wang J, Neaton J B, Zheng H, Nagarajan V, Ogale S B, Liu B, Viehland D, Vaithyanathan V, Schlom D G, Waghmare U V, Spaldin N A, Rabe K M, Wuttig M and Ramesh R 2003 *Science* **299** 1719
[9] Nan C W, Liu G and Lin Y H 2005 *Phys. Rev. Lett.* **94** 197203
[10] Qi X D, Dho J, Tomov R, Blamire M G and MacManus-Driscoll J L 2005 *Appl. Phys. Lett.* **86** 062903
[11] Palkar V R, Ganesh Kumara K and Malik S K 2004 *Appl. Phys. Lett.* **84** 2856
[12] Iakovlev S, Solterbeck C H, Kuhnke M and Es-Souni M 2005 *J. Appl. Phys.* **97** 094901
[13] Lee Y H, Wu J M, Chueh Y L and Chou L J 2005 *Appl. Phys. Lett.* **87** 172901
[14] Lee D, Kim M G, Ryu S, Jang H M and Lee S G 2005 *Appl. Phys. Lett.* **86** 222903
[15] Ederer C and Spaldin N A 2005 *Phys. Rev. B* **71** 060401
[16] Lin Y H, Jiang Q H, Wang Y and Nan C W 2007 *Appl. Phys. Lett.* **90** 172507
[17] Wang Y and Nan C W 2006 *Appl. Phys. Lett.* **89** 052903
[18] Neaton J B, Ederer C, Waghmare U V, Spaldin N A and Rabe K M 2005 *Phys. Rev. B* **71** 014113
[19] Lebeugle D, Colson D, Forget A and Viret M 2007 *Appl. Phys. Lett.* **91** 022907
[20] Wang S Y, Qiu X, Gao J, Feng Y, Su W N, Zheng J X, Yu D S and Li D J 2011 *Appl. Phys. Lett.* **98** 152902
[21] Huang A and Shannigrahi S R 2011 *J. Alloy. Compd.* **509** 2054
[22] Kogut I and Record M C 2013 *Intermetallics* **32** 184
[23] Kumar M, Yadav K L and Varma G D 2008 *Mater. Lett.* **62** 1159
[24] Mirabella S, Salvador D D, Napolitani E, Bruno E and Priolo F 2013 *J. Appl. Phys.* **113** 031101
[25] Kageshima H, Uematsu M and Shiraishi K 2001 *Microelectron. Eng.* **59** 301
[26] Cros A, Saoudi R, Hewett C A, Lau S S and Hollinger G 1990 *J. Appl. Phys.* **67** 1826
[27] Hedman J, Baer Y, Berndtsson A, Klasson M, Leonhardt G, Nilsson R, Nordling C 1972 *J. Electron Spectrosc. Relat. Phenom.* **1** 101
[28] Finster J, Klinkenberg E D, Heeg J and Braun W 1990 *Vacuum* **41** 1586
[29] Wang X L, Xiang J J, Wang W W, Zhang J, Han K, Yang H, Ma X L, Zhao C, Chen D P and Ye T C 2013 *Appl. Phys. Lett.* **102** 041603
[30] Mocioiu O C, Popa M, Neacsu E I and Zaharescu M 2013 *J. Non-Crystalline Solids* **361** 130